EPJ manuscript No.
(will be inserted by the editor)

Eulerian description of high-order bounce-back scheme for lattice Boltzmann equation with curved boundary

Taehun Lee[1,a] and Gary K. Leaf[2,b]

[1] Department of Mechanical Engineering, The City College of The City University of New York, New York, NY 10031, U.S.A.
[2] Mathematics and Computer Science Division, Argonne National Laboratory, Argonne, IL 60439, U.S.A.

Abstract. We propose an Eulerian description of the bounce-back boundary condition based on the high-order implicit time marching schemes to improve the accuracy of lattice Boltzmann simulation in the vicinity of curved boundary. The Eulerian description requires only one grid spacing between fluid nodes when the second-order accuracy in time and space is desired, although high-order accurate boundary conditions can be constructed on more grid-point support. The Eulerian description also provides an analytical framework for several different interpolation based boundary conditions. For instance, the semi-Lagrangian, linear interpolation boundary condition (Bouzidi *et al.* [Phys. Fluids **13**, 3452 (2001)]) is found to be a first-order upwind discretization that changes the time marching schemes from implicit to explicit as the distance between the fluid boundary node and the solid boundary increases.

1 Introduction

The most popular boundary condition for the lattice Boltzmann equation (LBE) method is the bounce-back scheme. In the standard bounce-back scheme, the incoming particle distribution function reflects back at the solid boundary during the streaming step, which makes the resolution of complex solid boundaries straightforward. Although simple to implement, it is only first-order accurate unless the solid boundary is located exactly half-way between the boundary fluid node and the off-lattice node inside the solid [1]. High-order boundary conditions for curved solid boundaries have been proposed to address this issue over the past decade [2–5]. Of particular interest is the interpolated bounce-back scheme proposed by Bouzidi *et al.* [2] for its stability and simple implementation. It is basically a method of backward characteristics; we move backward from the current fluid boundary node to search for the location where the particle distribution function at the previous time step resided. The accuracy of the scheme relies heavily on the interpolation scheme used to spatially approximate the value of the particle distribution function. While higher-order interpolations can easily improve the spatial accuracy, the scheme is inherently first-order accurate in time.

The goal of the present work is to present an alternative way to construct high-order bounce-back schemes. Instead of moving backward to find the previous location, we solve the pure

[a] e-mail: `thlee@ccny.cuny.edu`; This author was supported in part by the City University of New York under Contract PSC-CUNY 60084-37 38.
[b] e-mail: `leaf@mcs.anl.gov`; This author was supported by the U.S. Dept. of Energy under Contract DE-AC02-06CH11357.

advection equation at the fluid boundary nodes, noting that the streaming step is the exact solution of the pure advection equation. This not only enables use of high-order time and space discretizations on a given number of participating fluid boundary nodes but facilitate accuracy and stability analysis of the boundary conditions. This approach may be viewed as an Eulerian description of the bounce-back schemes, because the frame of reference is fixed at the fluid boundary nodes rather than it follows the particle distribution function.

The paper is organized as follows. In Sect. 2, derivation of LBE from the discrete Boltzmann equation (DBE) is presented. Sect. 3 begins with an Eulerian bounce-back scheme for curved boundaries. Detailed discretized forms of the first- and second-order accurate boundary conditions are examined. In Sect. 4, we apply the boundary conditions to the two-dimensional Couette flow to test the performance and characteristics of different boundary conditions. Concluding remarks are made in Sect. 5.

2 Lattice Boltzmann Equation

DBE with Bhatnagar-Gross-Krook (BGK) [6] model can be written as

$$\frac{\partial f_\alpha}{\partial t} + \mathbf{e}_\alpha \cdot \nabla f_\alpha = -\frac{f_\alpha - f_\alpha^{eq}}{\lambda} + \frac{(\mathbf{e}_\alpha - \mathbf{u}) \cdot \mathbf{F}_\alpha}{c_s^2} \Gamma_\alpha, \tag{1}$$

where f_α is the particle distribution function, $\mathbf{e}_\alpha$ is the microscopic particle velocity, $\mathbf{u}$ is the macroscopic velocity, ρ is the density, c_s is a constant, λ is the relaxation time, the equilibrium distribution function f_α^{eq} is given by

$$f_\alpha^{eq} = t_\alpha \rho \left[1 + \frac{\mathbf{e}_\alpha \cdot \mathbf{u}}{c_s^2} + \frac{(\mathbf{e}_\alpha \cdot \mathbf{u})^2}{2c_s^4} - \frac{(\mathbf{u} \cdot \mathbf{u})}{2c_s^2} \right], \tag{2}$$

t_α being a weighting factor, and $\Gamma_\alpha = f_\alpha^{eq}/\rho$. $\mathbf{F}_\alpha$ accounts for the momentum transfer at moving solid boundary in the direction of $\mathbf{e}_\alpha$ or averaged external forces such as gravity.

LBE is obtained by discretizing Eq. (1) along characteristics over the time step Δt: [7]

$$f_\alpha^{n+1}(\mathbf{j}) - f_\alpha^n(\mathbf{j} - \mathbf{e}_\alpha \Delta t) = -\int_t^{t+\Delta t} \frac{f_\alpha - f_\alpha^{eq}}{\lambda} dt' + \int_t^{t+\Delta t} \frac{(\mathbf{e}_\alpha - \mathbf{u}) \cdot \mathbf{F}_\alpha}{c_s^2} \Gamma_\alpha dt'. \tag{3}$$

The time integration in $[t, t + \Delta t]$ is coupled with the space integration in $[\mathbf{j} - \mathbf{e}_\alpha \Delta t, \mathbf{j}]$. Note that the discretization on the left-hand side of Eq. (3) is not unique, although it is the best approximation when $(\mathbf{j} - \mathbf{e}_\alpha \Delta t)$ falls exactly on the lattice node.

Suppose the solid boundary is located in $[\mathbf{j} - \mathbf{e}_\alpha \Delta t, \mathbf{j}]$ and the information on the unknown particle distribution is provided by a boundary condition. Application of the trapezoidal rule for second-order accuracy and unconditional stability leads to

$$\begin{aligned} f_\alpha^{n+1}(\mathbf{j}) - f_\alpha^n(\mathbf{j} - \mathbf{e}_\alpha \Delta t) = & -\tfrac{f_\alpha - f_\alpha^{eq}}{2\tau}\big|^n_{(\mathbf{j}-\mathbf{e}_\alpha \Delta t)} - \tfrac{f_\alpha - f_\alpha^{eq}}{2\tau}\big|^{n+1}_{(\mathbf{j})} \\ & + \tfrac{\Delta t}{2} \tfrac{(\mathbf{e}_\alpha - \mathbf{u}) \cdot \mathbf{F}_\alpha}{c_s^2} \Gamma_\alpha\big|^n_{(\mathbf{j}-\mathbf{e}_\alpha \Delta t)} + \tfrac{\Delta t}{2} \tfrac{(\mathbf{e}_\alpha - \mathbf{u}) \cdot \mathbf{F}_\alpha}{c_s^2} \Gamma_\alpha\big|^{n+1}_{(\mathbf{j})}, \end{aligned} \tag{4}$$

where the nondimensional relaxation time $\tau = \lambda/\Delta t$ and is related to the kinematic viscosity by $\nu = \tau c_s^2 \Delta t$.

Here, we introduce the modified particle distribution function $\bar{f}_\alpha$ and equilibrium distribution function $\bar{f}_\alpha^{eq}$ to facilitate computation:

$$\begin{aligned} \bar{f}_\alpha &= f_\alpha + \tfrac{f_\alpha - f_\alpha^{eq}}{2\tau} - \tfrac{\Delta t}{2} \tfrac{(\mathbf{e}_\alpha - \mathbf{u}) \cdot \mathbf{F}_\alpha}{c_s^2} \Gamma_\alpha, \\ \bar{f}_\alpha^{eq} &= \quad f_\alpha^{eq} - \tfrac{\Delta t}{2} \tfrac{(\mathbf{e}_\alpha - \mathbf{u}) \cdot \mathbf{F}_\alpha}{c_s^2} \Gamma_\alpha. \end{aligned} \tag{5}$$

Eq. (5) can then be recast in a simpler form:

$$\bar{f}_\alpha^{n+1}(\mathbf{j}) - \bar{f}_\alpha^{n}(\mathbf{j}-\mathbf{e}_\alpha \Delta t) = -\frac{1}{\tau+0.5}\left(\bar{f}_\alpha - \bar{f}_\alpha^{eq}\right)|^n_{(\mathbf{j}-\mathbf{e}_\alpha\Delta t)} + \Delta t \frac{(\mathbf{e}_\alpha-\mathbf{u})\cdot\mathbf{F}_\alpha}{c_s^2}\Gamma_\alpha|^n_{(\mathbf{j}-\mathbf{e}_\alpha\Delta t)}, \quad (6)$$

where the nondimensional relaxation time $\tau = \lambda/\Delta t$ and is related to the kinematic viscosity by $\nu = \tau c_s^2 \Delta t$. We note that although Eq. (6) appears to be explicit in time, it is fully implicit for the relaxation term and the intermolecular force terms alike and, therefore, is unconditionally stable and second-order accurate. Eq. (6) is solved in two steps away from solid boundaries:

Collision step

$$\bar{f}_\alpha^{n}(\mathbf{j}-\mathbf{e}_\alpha\Delta t) = \bar{f}_\alpha^{n}(\mathbf{j}-\mathbf{e}_\alpha\Delta t) - \frac{\bar{f}_\alpha - \bar{f}_\alpha^{eq}}{\tau+0.5}|^n_{(\mathbf{j}-\mathbf{e}_\alpha\Delta t)} + \Delta t\frac{(\mathbf{e}_\alpha-\mathbf{u})\cdot\mathbf{F}_\alpha}{c_s^2}\Gamma_\alpha|^n_{(\mathbf{j}-\mathbf{e}_\alpha\Delta t)} \quad (7)$$

Streaming step

$$\bar{f}_\alpha^{n+1}(\mathbf{j}) = \bar{f}_\alpha^{n}(\mathbf{j}-\mathbf{e}_\alpha\Delta t). \quad (8)$$

The density and the momentum can be computed by taking the zeroth and first moments of the modified particle distribution function:

$$\begin{aligned} \rho &= \textstyle\sum_\alpha \bar{f}_\alpha, \\ \rho\mathbf{u} &= \textstyle\sum_\alpha \mathbf{e}_\alpha \bar{f}_\alpha + \frac{\Delta t}{2}\sum_\alpha \mathbf{F}_\alpha. \end{aligned} \quad (9)$$

The streaming step can be regarded as a Lagrangian approach in that a group of particles represented by the particle distribution function move along characteristics [8]. The perfect shift poses no stability and accuracy issues because it involves neither phase nor amplitude error. Since the perfect shift is the exact solution of the pure advection equation, the Lagrangian description given by Eq. (8) can alternatively be expressed in an Eulerian framework shown below

$$\frac{\partial \bar{f}_\alpha}{\partial t} + \mathbf{e}_\alpha \nabla \bar{f}_\alpha = 0. \quad (10)$$

Second-order accurate advection schemes need to be used to discretize Eq. (10) in order to maintain the overall second-order accuracy of the LBE method. The bar for the particle distribution function will be dropped hereinafter.

3 Curved Boundary Conditions

Fig. 1(a) shows the schematics of bounce-back boundary conditions in the direction of the microscopic velocity $\mathbf{e}_\alpha$. It is desired that the particle distribution function f_α at the boundary fluid node $\mathbf{j}$ is calculated from the particle distribution function f_{α^*} moving in the opposite direction under the assumption that it is reflected back at the solid boundary. q is the dimensionless distance between the boundary fluid node and the solid boundary. The standard link bounce back scheme is realized for $q = 1/2$, in which case the solid boundary is located half way between the boundary fluid node $\mathbf{j}$ and the off-lattice location $\mathbf{j} - \mathbf{e}_\alpha\Delta t$. For $q \neq 1/2$, interpolation needs to be introduced. Bouzidi *et al.* [2] proposed the interpolated bounce-back schemes based on the method of characteristics. From the geometrical point of view, we move backward from the node $\mathbf{j}$ relative to the particle distribution function f_α and locate the position that f_α sat on at the previous time step. Once the location is found, f_α can be interpolated with the values at the neighboring nodes.

Alternatively, we place an imaginary node at $(\mathbf{j} - 2q\Delta x)$ inside the solid, which is separated from the node $(\mathbf{j})$ by $2q\Delta x$ and is a reflection of the node $(\mathbf{j})$ around the solid boundary as illustrated in Fig. 1(b). The presence of the solid boundary is ignored. Accordingly, $f_\alpha(\mathbf{j}-2q\Delta x)$ is identical to $f_{\alpha^*}(\mathbf{j})$ and is assumed to continuously vary as it travels past the solid boundary. With two grid points and continuity of the solution, the standard time and space discretizations can be applied to Eq. (10).

3.1 First-order accurate schemes in space

Application of the finite difference approximation to Eq. (10) with two grid points ($\mathbf{j}$) and ($\mathbf{j} - 2q\Delta x$) yields the first order accurate schemes in space.

$$[2qf_\alpha^{n+1}(\mathbf{j}) - 2qf_\alpha^n(\mathbf{j})] = -(1-\theta)[f_\alpha^{n+1}(\mathbf{j}) - f_\alpha^{n+1}(\mathbf{j} - 2q\Delta x)] - \theta[f_\alpha^n(\mathbf{j}) - f_\alpha^n(\mathbf{j} - 2q\Delta x)], \quad (11)$$

where $\theta = [0, 1]$ and $\mathbf{e}\Delta t/\Delta x = 1$ is assumed. For $\theta = 1$, the scheme reduces to the explicit upwind scheme but can be singular as q approaches zero. The maximum stable θ is found to be $\theta = min(1, 2q)$, for which Eq. (11) becomes

$$f_\alpha^{n+1}(\mathbf{j}) = \begin{cases} f_\alpha^n(\mathbf{j}) - \frac{(1-2q)}{2q}[f_\alpha^{n+1}(\mathbf{j}) - f_\alpha^{n+1}(\mathbf{j} - 2q\Delta x)] - [f_\alpha^n(\mathbf{j}) - f_\alpha^n(\mathbf{j} - 2q\Delta x)], & q < \frac{1}{2}, \\ f_\alpha^n(\mathbf{j}) - \frac{1}{2q}[f_\alpha^n(\mathbf{j}) - f_\alpha^n(\mathbf{j} - 2q\Delta x)], & q > \frac{1}{2}. \end{cases} \quad (12)$$

Eq. (12) is the implicit upwind with respect to the microscopic velocity $\mathbf{e}_\alpha$ when $q < 1/2$ and explicit upwind when $q > 1/2$. By noting that the grid point ($\mathbf{j} - 2q\Delta x$) is a mere reflection of a point ($\mathbf{j}$), and $f_\alpha(\mathbf{j} - 2q\Delta x)$ is equivalent to $f_{\alpha^*}(\mathbf{j})$, Eq. (12) can be expressed with the unknowns at the single fluid boundary node ($\mathbf{j}$);

$$f_\alpha^{n+1}(\mathbf{j}) = \begin{cases} 2qf_{\alpha^*}^n(\mathbf{j}) + (1-2q)f_{\alpha^*}^{n+1}(\mathbf{j}), & q < \frac{1}{2}, \\ \frac{1}{2q}f_{\alpha^*}^n(\mathbf{j}) + \frac{(2q-1)}{2q}f_\alpha^n(\mathbf{j}), & q > \frac{1}{2}. \end{cases} \quad (13)$$

It is interesting to note that Eq. (13) is the linear interpolation scheme of Bouzidi *et al.* [2] due to $f_{\alpha^*}^{n+1}(\mathbf{j}) = f_{\alpha^*}^n(\mathbf{j} - \mathbf{e}_{\alpha^*}\Delta t)$. Therefore, the linear interpolation scheme of Bouzidi *et al.* behaves like a first-order upwind discretization that changes the time marching schemes from implicit to explicit as the distance between the fluid boundary node and the solid boundary increases.

In general, solving for $f_\alpha^{n+1}(\mathbf{j})$ gives

$$f_\alpha^{n+1}(\mathbf{j}) = \frac{\theta}{(2q+1-\theta)}f_{\alpha^*}^n(\mathbf{j}) + \frac{(1-\theta)}{(2q+1-\theta)}f_{\alpha^*}^{n+1}(\mathbf{j}) + \frac{(2q-\theta)}{(2q+1-\theta)}f_\alpha^n(\mathbf{j}). \quad (14)$$

Eq. (14) becomes second-order accurate in time only if $\theta = 1/2$ (mid-point rule), but still remains first-order accurate in space.

3.2 Second-order accurate schemes in space

To derive second-order accurate schemes, the linear Galerkin finite element approximation is applied to Eq. (10) for two grid points ($\mathbf{j}$) and ($\mathbf{j} - 2q\Delta x$) [9].

$$\begin{aligned} &[\tfrac{4q}{3}f_\alpha^{n+1}(\mathbf{j}) + \tfrac{2q}{3}f_{\alpha^*}^{n+1}(\mathbf{j})] - [\tfrac{4q}{3}f_\alpha^n(\mathbf{j}) + \tfrac{2q}{3}f_{\alpha^*}^n(\mathbf{j})] \\ &= -(1-\theta)[f_\alpha^{n+1}(\mathbf{j}) - f_{\alpha^*}^{n+1}(\mathbf{j})] - \theta[f_\alpha^n(\mathbf{j}) - f_{\alpha^*}^n(\mathbf{j})], \end{aligned} \quad (15)$$

where $\theta = [0, 1]$. Solving for $f_\alpha^{n+1}(\mathbf{j})$ gives

$$f_\alpha^{n+1}(\mathbf{j}) = \frac{(2q+3\theta)}{(4q+3-3\theta)}f_{\alpha^*}^n(\mathbf{j}) + \frac{(3-3\theta-2q)}{(4q+3-3\theta)}f_{\alpha^*}^{n+1}(\mathbf{j}) + \frac{(4q-3\theta)}{(4q+3-3\theta)}f_\alpha^n(\mathbf{j}). \quad (16)$$

For $\theta = 1/2$, Eq. (16) is second-order accurate both in time and space. The maximum stable θ for the second-order schemes is then $\theta = min(2/3, 4q/3)$.

$$f_\alpha^{n+1}(\mathbf{j}) = \begin{cases} 2qf_{\alpha^*}^n(\mathbf{j}) + (1-2q)f_{\alpha^*}^{n+1}(\mathbf{j}), & q < \frac{1}{2}, \\ \frac{2q+2}{4q+1}f_{\alpha^*}^n(\mathbf{j}) + \frac{1-2q}{4q+1}f_{\alpha^*}^{n+1}(\mathbf{j}) + \frac{4q-2}{4q+1}f_\alpha^n(\mathbf{j}), & q > \frac{1}{2}. \end{cases} \quad (17)$$

4 Numerical Test

We carry out a simple test for the unsteady Couette flow, for which the analytical solution is available. Fig. 2 shows the error of the difference boundary conditions versus the distance p from the solid boundary. Periodic boundary conditions are prescribed in the horizontal direction and 40 grid points are used in the vertical direction. The top boundary is moving at constant speed. The nondimensional relaxation time is fixed at $\tau = 1/2$. The line with filled square is the result obtained by using the linear scheme of Bouzidi *et al.* For q less than $1/2$, the error decreases fast as the distance increases. This regime corresponds the implicit upwind. The error then stays at approximately the same value but abruptly increases as q approaches unity. It is clear that the linear interpolation scheme is discontinuous at $q = 1$ and non-smooth at $q = 1/2$, which may give rise to oscillations in the stress distribution along the curved boundary. The line with filled delta is the result obtained by using the second order scheme in space and time Eq. (16). It has slightly higher error than the linear scheme of Bouzidi *et al.*, but the error is continuous at $q = 1$ and smooth at $q = 1/2$. The line with filled gradient is the result obtained by using the scheme Eq. (12) that is first order in space and second order in time. It has higher error than the linear scheme of Bouzidi *et al.*, but the error exhibits smooth behavior. The line with hollow circle is the result from the scheme that is second order in space but first order in time, which also has discontinuity at $q = 1$.

Generally, the error of both first- and second-order schemes is reduced as $\theta \to 1$, *i.e.*, as the scheme becomes more explicit in time, in which case the scheme is only conditionally stable for $\theta < 1/2$ and the maximum stable θ becomes a function of the distance from the boundary. The second-order schemes slightly better perform than the first-order schemes at the same θ in terms of accuracy. The choice of $\theta = 1/2$ results in second-order accuracy in time and provides smooth solution at $q = 1/2$ and continuous solution at $q = 1$.

5 Concluding Remarks

By applying the general time marching scheme to the streaming step, we were able to construct both first- and second-order accurate bounce-back schemes for curved boundaries. The first-order schemes were derived by applying the standard finite difference approximation, and the second-order schemes were derived by applying the Galerkin finite element approximation in one-dimension. It has been shown that the linear scheme of Bouzidi *et al.* is a special case of the first-order accurate schemes, which changes its type from implicit to explicit as the distance between the fluid node and the boundary increases. This causes non-smooth and discontinuous transition in the error distribution and may lead to oscillations in the stress field along the curved boundary. Numerical test suggests that the fixed time marching scheme, in particular, the mid-point rule performs better in terms of smoothness and continuity in the error distribution.

References

1. X. He, Q. Zou, L.-S. Luo, and M. Dembo, J. Stat. Phys. **87**, (1997) 115
2. M. Bouzidi, M. Firdaouss, and P. Lallemand, Phys. Fluids **13**, (2001) 3452
3. R. Mei, L.-S. Luo, and W. Shyy, J. Comput. Phys. **155**, (1999) 307
4. I. Ginzburg, D. d'Humières, Phys. Rev. E **68**, (2003) 066614
5. M. Junk and Z. Yang, Phys. Rev. E **72**, (2005) 066701
6. H. Chen, S. Chen, and W.H. Matthaeus, Phys. Rev. A **45**, (1992) 5339
7. T. Lee and P.F. Fischer, Phys. Rev. E **74**, (2006) 046709
8. T. Lee and C.-L. Lin, J. Comput. Phys. **185**, (2003) 445
9. P.M. Gresho and R.L. Sani, *Incompressible Flow and the Finite Element Method* (Wiley, 1998)

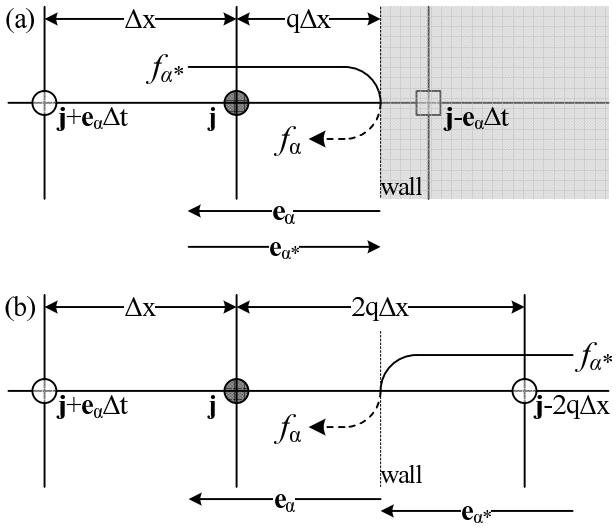

Fig. 1. (a) Schematic of the interpolated boundary conditions in the direction of $\mathbf{e}_\alpha$. ($\mathbf{j}$) is the fluid boundary node and ($\mathbf{j} - \mathbf{e}_\alpha \Delta t$) is the off-lattice node. (b) $f_\alpha(\mathbf{j} - 2q\Delta x)$ is a reflection of $f_{\alpha^*}(\mathbf{j})$.

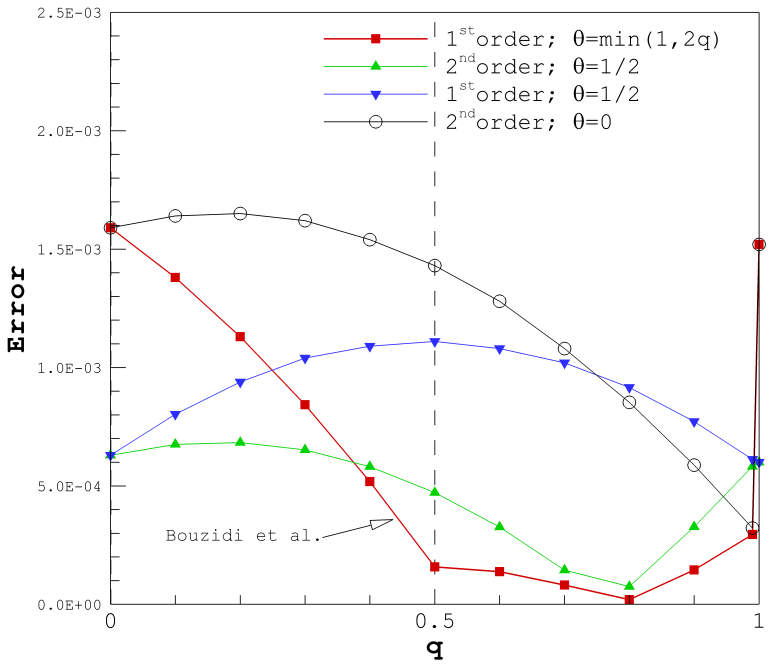

Fig. 2. L1 norm versus the distance q from the solid boundary.